scientific reports

Check for updates

OPEN

Quantitative analysis of the performance improvement of the surrounding rock mass by applying a prestressed bolt system

Xuxu Yang, Hongyun Xue, Junwei Guo✉ & Mingming Zhang

Prestressed bolts have been increasingly used in underground engineering as a practical solution to control the instability of surrounding rock masses. However, blindly increasing the density of prestressed bolt has limited influence on the performance improvement of tunnel surrounding rock mass. Therefore, the accurate design of the parameters of the prestressed bolt in the support system is a significant method to improve the bearing capacity of the tunnel surrounding rock. To solve this problem, we carried out large-scale physical model tests of anchored rock block with nonpersistent joints. An innovative method for prestressed bolt simulation is proposed by using the code independently developed in PFC^{3D}, and then a series of numerical model compression tests of anchored rock block with different prestressed bolt densities are extended based on physical model tests. The results indicate that the original failure mode of the rock block is not changed by adding bolt. And an increase in the density of the prestressed bolt leads to a change in the anchoring mechanism of the rock block. When the density of prestressed bolt is low, the upper load is mainly borne by rock block, and the increase of the density of bolt will mobilize more intact rock to participate in the load. When the density of prestressed bolt increases to a certain extent, the upper load is mainly borne by the prestressed bolt. And the performance improvement of prestressed bolt to rock block is limited. When the prestress and density of bolt reach a certain degree, the strength of rock mass is only increased by 10% when the prestress and density of bolt are doubled. The increase of the density of prestressed bolt makes the deformation of rock block more stable, and the $\varepsilon_3/\varepsilon_1$ ratio of the anchored rock block is always less than 1.0. The research results have important guiding significance for tunnel surrounding rock masses support design.

Keywords Anchored rock blocks, Compression tests, Prestressed bolt system, PFC^{3D}, Support design

Tunnel excavation disturbs the original stress balance state of the surrounding rock mass[1], leading to the release of the deformation energy that results in the displacement of the surrounding rock masses. Fracture occurs when the deformation limit of the surrounding rock mass is exceeded, and the slip of the rock blocks along the joint and fracture plane leads to instability of the surrounding rock masses[2]. To date, tunnel engineering has extensively employed bolts and their application is a key supporting method in underground engineering[3,4]. Bolt support can maintain the integrity and stability of surrounding rock to the maximum extent, manage the progression of deformation, displacement and fracture of surrounding rock, so as to improve the stability of tunnel surrounding rock. However, non-prestressed bolt support is passive support, which is difficult to "actively and quickly improve" the stress state of tunnel surrounding rock mass and "actively mobilize and facilitate" the bearing capacity of surrounding rock mass.

By employing prestress to the bolt, the bolt can maintain a part of the surrounding rock mass under compression. This improves the mechanical properties of the anchoring system, inhibits the bending deformation of the surrounding rock mass, and limits the occurrence of tensile and shear failure of the surrounding rock mass, actively mobilizing the bearing capacity of the surrounding rock mass, and improving the stability of underground engineering[5,6]. At present, the research results of the influence of prestressed bolt on the mechanical properties of rock mass are relatively abundant. Table 1 shows the research progress in the application of prestressed bolt to rock mass reinforcement.

Shandong Key Laboratory of Civil Engineering Disaster Prevention and Mitigation, Shandong University of Science and Technology, Qingdao 266590, China. ✉email: 202082040010@sdust.edu.cn

Research progress of prestressed bolt	References
The improvement of mechanical parameters such as peak strength, deformation modulus, cohesion and friction angle after bolt reinforcement	7,8
The load transfer mechanism between the bolts and rock masses	9,10
The stress evolution law of bolts during the deformation of rock masses	11–14
Bolt reinforcement effect for rock masses under different joint types	15–17
Reinforcement mechanism and optimization of bolts	7,18,19
A three-stage shear deformation model of anchor bolts	20
The bolt reinforcement of rock masses with secondary failure	21

Table 1. The research progress in the application of prestressed bolt to rock mass reinforcement.

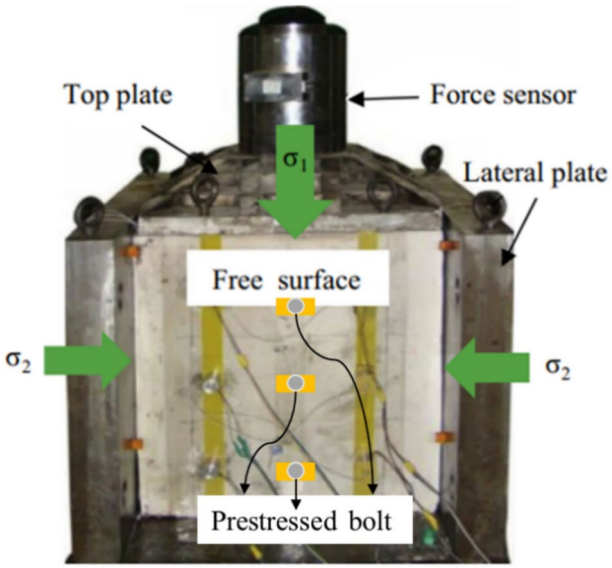

Fig. 1. Large scale 3D bolt reinforcement of rock masses physical test.

These studies have focused on the anchoring influence of a single prestressed bolt on the rock mass and did not investigate the performance improvement of the prestressed bolt system for the rock masses surrounding the tunnel. However, in tunnel engineering, particularly for surrounding rock masses with fracture development, even when a single bolt fails, other bolts in the bolt system can still significantly provide the bearing capacity of the surrounding rock masses[22]. Therefore, it is crucial to study the improvement in the performance of the prestressed bolt system for the rock masses surrounding tunnels, further explore the influence of prestressed bolt density on the performance improvement of rock masses.

On the basis of the project background of the Shishan Road station of Qingdao Metro Line 6, the surrounding jointed rock mass separated from the tunnel was chosen as the research object. We have carried out large-scale physical tests of anchored rock block with nonpersistent joints. And a new prestressed bolt simulation method was proposed through self-developed code in PFC^{3D}. Then the physical test was further extended to quantitatively analyze the relationship between the prestress and density of bolt and the strength, deformation and failure mode of rock mass. Explore the limiting effect of prestressed bolt on the performance improvement of rock mass. This study can provide important guidance for the design of similar projects.

Establishment of the numerical model

Setup of the PFC^{3D} numerical model

To quantitatively study the anchoring effect of rock masses surrounding tunnels, a numerical simulation study was carried out based on the experimental studies on large-scale synthetic jointed rock blocks conducted by Jing et al.[23] The rock mass with the dimensions of 2.5 m × 2.5 m × 2.5 m and containing preexisting nonpersistent joints was separated from the surrounding rock mass of tunnel excavation as the research object. Figure 1 shows the large-scale three-dimensional rock mass bolt reinforcement simulation test system. The top surface is used to apply pressure loads, and the bottom surface remains stationary vertically. The opposite side of the free surface is fixed in the horizontal direction and does not displace during the test. The displacement control was adopted to realize uniaxial loading of the sample, and the speed was 0.03 mm/min. The size of the physical test model is 0.5 m × 0.5 m × 0.5 m to simulate the surrounding rock mass with the size of 2.5 m × 2.5 m × 2.5 m in the actual project[24,25]. The mechanical parameters of the physical experiment model are presented in Table 2.

Parameter	Volume weight (kN/m^{-3})	Young's modulus (GPa)	Compressive strength (MPa)	Tensile strength (MPa)	Poisson's ratio	Friction angle(°)
Physical model	17.05	1.79	7.32	0.57	0.16	33.5

Table 2. Mechanical parameters of the physical experiment model.

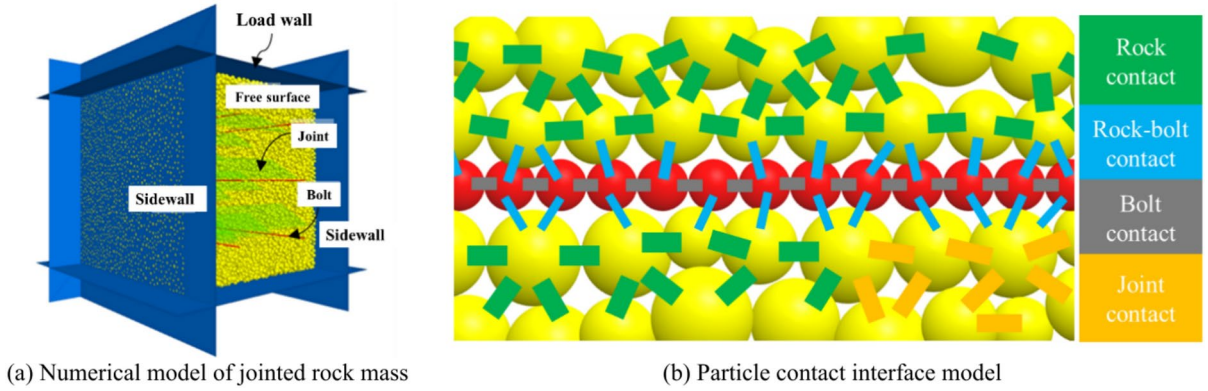

Fig. 2. Numerical model of a jointed rock mass with bolts.

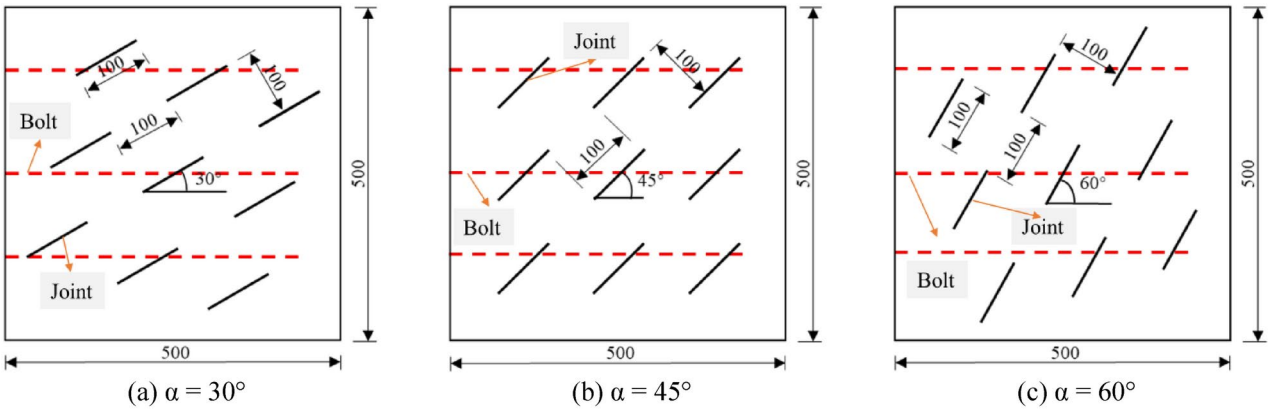

Fig. 3. Layout of joints and bolts.

Parameter	Young's modulus (GPa)	Yield strength (MPa)	Elongation (%)
Bolt	210	400	≥ 16

Table 3. Parameters of the bolt.

The numerical model of jointed rock blocks is shown in Fig. 2a. The dimensions of the model are 500 mm × 500 mm × 500 mm, and the model contains nine nonpersistent joints, which are arranged en echelon and are symmetrical, and the dip angles are 30°, 45° and 60°. Each joint's length is 100 mm, the length of the rock bridge between adjacent joints is 100 mm, and the joint spacing between parallel joints is 100 mm. A single-row bolt is applied to the sample, as shown in Fig. 3. The bolt reinforcement length is 440 mm. Full-length bonded anchoring is adopted, and epoxy resin is used as an anchoring agent to reinforce the bolt. The parameters of the bolt are shown in Table 3. In this study, the results obtained from physical model tests are used to determine and confirm the parameters of the numerical model.

The parallel-bond model (PBM) can transmit both force and moment at the same time, which can better reflect the mechanical properties of intact rock. Joints observed by field joint information collection are mostly closed, and there is no weak interlayer between the joints, so it can be approximated that only sliding friction along the joint direction exists between the rock masses on both sides of the joints. In the numerical model, the PBM is used for the contact of the intact rock (the green lines in Fig. 2b), and the smooth-joint model (SJM)

is used for the contact model of the joints (the yellow lines in Fig. 2b). Particles with a diameter of 4.0 mm are arranged outward to form the bolt element. The bolt particles are added after the formation of the intact rock model, and a bolt hole with a diameter of 6.0 mm is generated by removing the rock particles. Then, the particles are cut from each other and arranged in turn by "Loop" to generate model bolts. The linear-bond model (LBM) is used for the contact of the bolt particles and the rock-bolt interface (shown by blue and dark lines in Fig. 2b).

To fully reflect the mechanical properties of rock blocks, it is vital to calibrate the microscopic parameters of the numerical model. The "trial and error" approach was used to settle the parameters of the numerical model; that is, the microscopic parameters (input parameters) are constantly adjusted until the macroscopic mechanical parameters of the numerical model match the results obtained by physical experiment model[26–28]. The model parameters determined by the "trial and error" approach are shown in Table 4.

Methodology development of the prestressed bolt

Currently, prestressed bolts are mostly simulated using the FLAC^{3D} and 3DEC software[29–31]. However, these methods analyze tunnel stability from a macroscopic perspective. Few studies on the anchoring effect of prestressed bolts have been performed using the PFC^{3D} particle flow discrete element software, and most researchers have studied only the generation method of bolts using PFC^{3D}[32]. Wang et al.[33] applied prestress of the bolt by moving the tray at the end of the bolt. However, PFC corresponds to the transfer of force through contact between entities (particles, clusters, walls); if a wall is used to simulate a tray in the model, sufficient contact between the wall and the particles is needed. In the numerical model of this study, due to the limitation of the particle size of the bolt, there are only a few contacts between the generated wall and the bolt particles, and it is difficult to obtain an effective force. The function of the tray in prestressed anchorage is to limit the relative movement between the interface of the bolt and rock. Therefore, by implemented a program written in the FISH language to increase the contact mechanics parameters between the end particles of the bolt and the rock mass particles, prestressed bolt reinforcement can also be realized. Figure 4 shows the force chain diagram of the contact force of the sample after the prestress is applied. In the figure, the size of the contact force is symbolized by the size of the column, while blue represents compression, and green represents tension. Figure 4 shows that the whole bolt is in a state of tension, the tension along the length of the bolt is reduced, and the strengthened contact of the bolt end and the nearby rock particles is due to compression. This method can accurately reflect the stress of a prestressed bolt.

Validation of numerical model

Figure 5 shows the results of the physical experiment compared with the numerical model with single-row bolts under different joint dip angles. For $\alpha = 30°$, the failure of the physical experiment model is composed of tensile fracture of the inner tip of joint 1 and secondary coplanar fracture of the outer tips of Joints 1, 3 and 6, forming a "step type" macroscopic fracture plane. The numerical model with $\alpha = 30°$ also produces a "step type" failure mode.

For $\alpha = 45°$, the failure path is mainly composed of coplanar joints 4 and 5, which are connected with Joint 8 after turning. Moreover, another macroscopic failure plane is formed by the tensile fracture of the inner tip of Joint 7, which cuts through the rock bridge between the outer tips of Joint 7 and Joint 9. In addition, a triangular failure zone is formed by joints 1, 3 and 6 at the right end of the rock block, and the intersection point of the triangular failure zone is located in the middle bolt. The corresponding numerical model displays a failure mode similar to the physical experiment.

For $\alpha = 60°$, the triangular failure zone is composed of joints 1 and 3, and the slip fracture planes along joints 4, 5 and 6 form at the right end of the rock mass. These failure modes are also reflected in the corresponding numerical model. Thus, comparison of numerical and physical model results shows that the calibrated numerical

Object	Parameter	Value
Intact rock contact (PBM)	Effective modulus, (GPa)	0.36
	Stiffness ratio	1.7
	Tensile strength, (MPa)	0.95
	Cohesive strength, (MPa)	0.38
	Friction coefficient	0.58
Bolt contact (LBM)	Effective modulus, (GPa)	1.17
	Stiffness ratio	1.5
	Friction coefficient	0.42
Rock-bolt contact (LBM)	Effective modulus, (GPa)	0.16
	Stiffness ratio	1.5
	Friction coefficient	0.42
Joint contact (SJM)	Normal stiffness, (N/m^3)	0.58×10^9
	Shear stiffness, (N/m^3)	0.21×10^9
	Particle friction coefficient	0.40

Table 4. Parameters of the jointed rock mass with bolts.

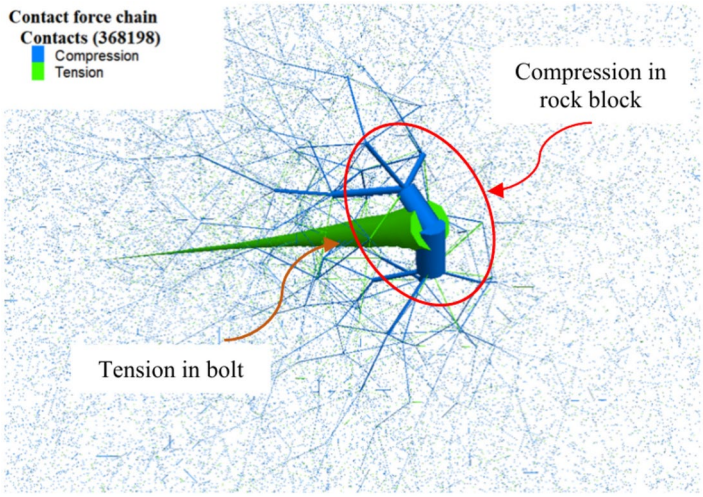

Fig. 4. Application of bolt prestress.

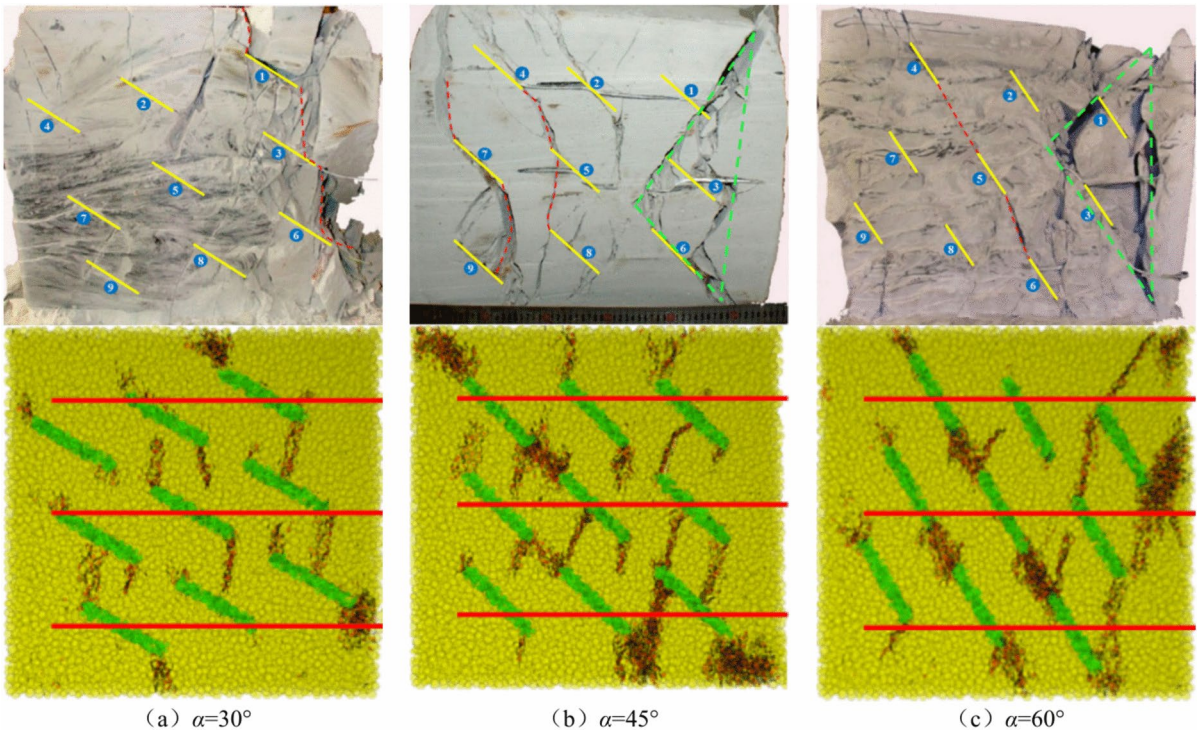

Fig. 5. Comparison of failure images of rock blocks with single-row bolt.

model can accurately obtain the failure mode generated in the physical experiments under the same conditions. The comparison results of the above models show the precision of the numerical model established in the study.

To further confirm the rationality of the prestressed bolt simulation method proposed in this study, using the method for the application of bolt prestress described in Sect."Methodology development of the prestressed bolt", the influence of different prestresses on the mechanical performance of rock blocks is further explored. A single-row anchored rock block with a joint dip angle of 60° is selected, and different prestresses of 0, 0.2, 0.4 and 0.6 kN are applied to the bolt. The stress–strain relationship of the sample under each prestress is shown in Fig. 6.

It is found that the prestress clearly influences the peak strength of a sample and is positively correlated with the peak strength. When the prestress of the bolt is 0, the bolt peak strength is 4.74 MPa, whereas the peak strengths of the samples with prestresses of 0.2, 0.4 and 0.6 kN are 7.48, 8.97 and 9.55 MPa, respectively. This shows that increasing the prestress increases the bearing capacity of the sample, and with increasing prestress, the rate of increase in the peak strength decreases. When the prestress increases from 0.4 kN to 0.6 kN, the

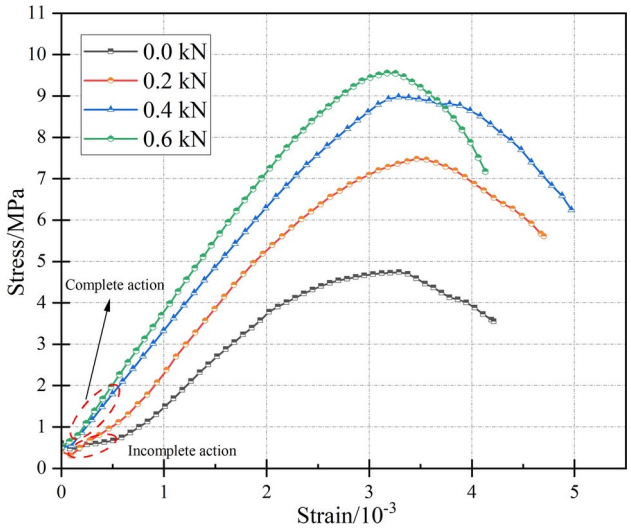

Fig. 6. Stress–strain curves of anchored rock blocks under different prestress.

corresponding peak strength only increases by 6.5%. Under full-length bolt reinforcement, the extent of the active support range to the interior of the model increases with larger prestress.

Under low prestress, the strength increase rate of the samples at the initial loading stage gradually becomes stable with increasing load and enters the linear elastic increase stage, indicating that the role of the bolt at the initial loading stage gradually becomes prominent. Increasing the prestress can significantly reduce the lag of the action of the bolt. When the prestress is applied to 0.4 kN, it enters the elastic stage initially of loading, and the stress–strain curve is linear. The results display that for a jointed rock mass, the bolt plays a strengthening role from the beginning of loading, and the prestress affects the time of full action of the bolt. It is worth noting that the time of full action of bolt is that the growth rate of bolt stress with strain is always at the maximum. The integrity of the bolt and rock mass, and the deformation resistance of the sample increase with greater prestress. Due to the constant loading rate of the model, the time for the bolt to reach the ultimate strength decreases with greater prestress. Taking the sample with a prestress of 0.6 kN as an example, the high prestress causes the force of the bolt to increase rapidly to yield failure, the sample reaches the peak strength at the earliest time among the studied samples, and the curve after the peak drops rapidly.

Results and analysis

To date, many scholars have used tunnel engineering as the research object for the study of prestressed bolt system[34], and have used qualitative methods to examine the control effect of prestressed bolt systems on the rock masses surrounding tunnels[35]. To further quantitatively investigate the performance improvement effect of the prestressed bolt system on surrounding rock masses, we carried out a series of compression tests on nonpersistent jointed rock blocks with different prestressed bolt densities. We take a rock block with a joint dip angle of 60° as the research object, and the prestress of the bolt is set to 0.4 kN. The bolt system density is set to no bolt, single-row, double-row and triple-row.

Influence of the prestressed bolt density on the failure mode of jointed rock blocks

Numerical compression tests are performed on rock blocks, focusing on various prestressed bolt densities through a series of model experiments. For each condition, four failure images at different stress–strain stages are listed in Fig. 7. The first is the image of the rock block at the beginning of the microscopic fractures in the compression process. The second is the image of the rock block when the stress reaches its peak strength during the compression process; that is, $\sigma_1 = \sigma_p$. The third is the image of the rock block when the stress is $0.85\sigma_p$ at the post-peak stage in the compression process. The fourth is the image of the rock block when the stress is $0.7\sigma_p$ at the post-peak stage in the compression process. In addition, to further explore the failure process of rock block during the compression process, the displacement diagrams of the above four stages are listed in Fig. 7.

It is evident from Fig. 7 that the rock pillar between the joint normal directions will slip along the joint dip angle under loading, and the rock bridge between the joint dip direction will hinder the movement of the rock pillar, so that the displacement of the model as a whole shows a trend of gradually decreasing from the bottom right to the top left, forming a step displacement diagram. This feature is the most obvious for double-row bolts. Further analysis shows that the two rock bridges between joints 4, 5 and 6 hinder the sliding trend of the whole rock block on the right side of the above three joints, resulting in fractures first and concentrated on the development of the tips of joints 4, 5 and 6. After the peak, fractures basically penetrate the three joints in a straight line, forming the main macroscopic slip plane. The sliding plane is more obvious in single-row and triple-row bolts reinforcement, but the anchoring effect is completely different. When single-row bolts reinforcement, the bolt at the intersection of the sliding plane is subjected to shear yield, and the right wedge-shaped block cannot support the axial load under the anchoring of the three broken bars. The wedge-shaped

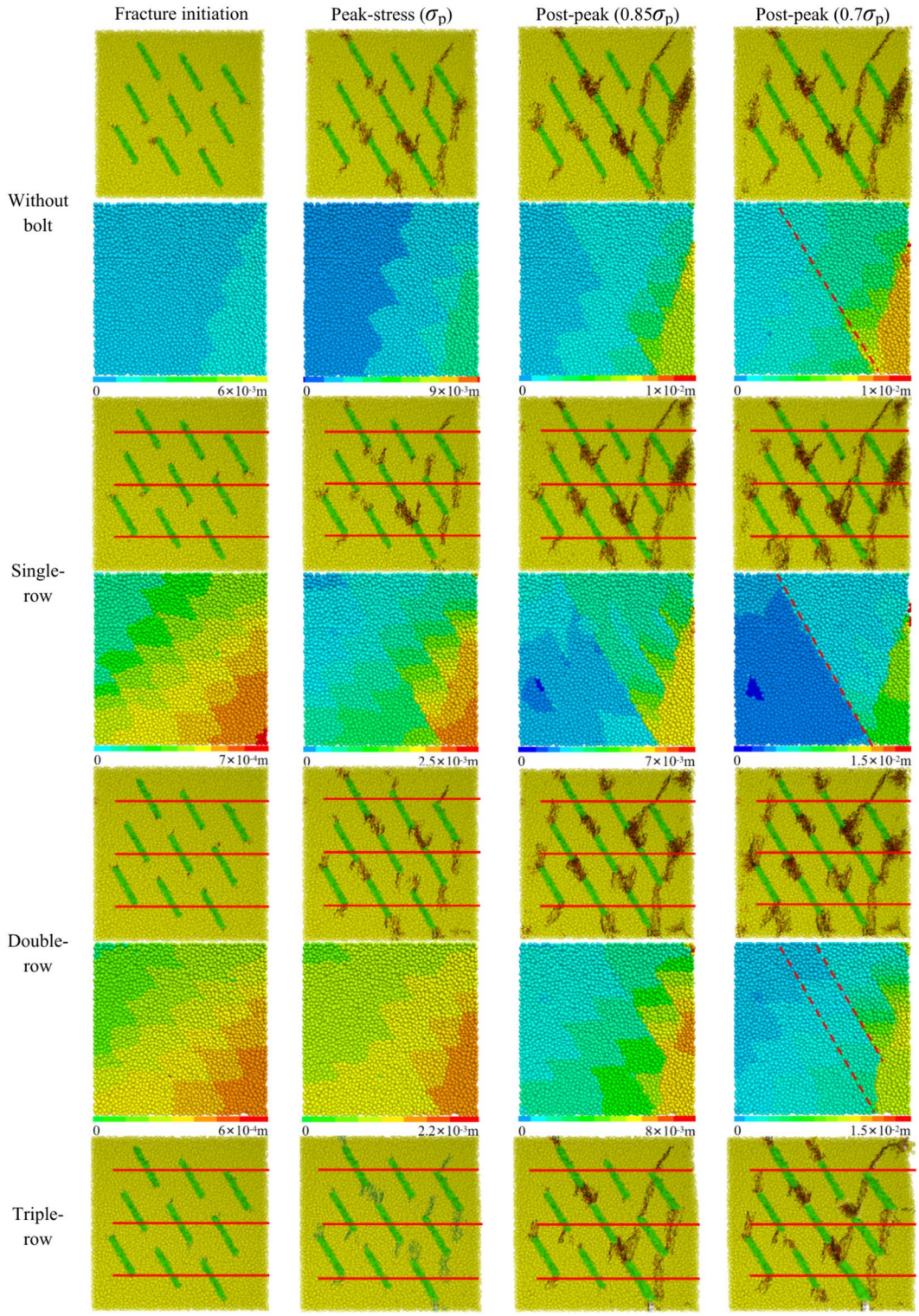

Fig. 7. Particle displacement and fracture propagation in 60° jointed rock blocks.

rock block is divided into triangular and quadrilateral blocks along the outer ends of joints 1, 3 and 6. When triple-row bolts reinforcement, due to the large density of the bolt, the bolt is sufficient to withstand the tensile shear load at the fracture plane, resulting in the right side of the model to slide along the bolt without losing stability under anchoring. The load is mainly borne by the bolt, and the failure degree of the rock block on the left side is reduced. The double-row anchored rock block can mobilize more intact rock to participate in the load bearing, and the fractures at the joint tip are generally developed, and more slip planes are formed along the dip angle, and the main control slip plane is not obvious. In a world, anchoring did not change the original failure

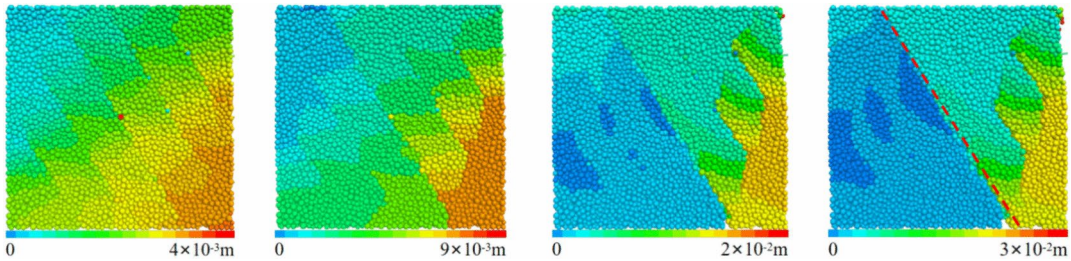

Figure 7. (continued)

mode of the rock block. The final failure mode of the rock block with bolt was more broken than that of the rock block without bolt. Secondary failure occurred in the rock block near the free surface, the stress shifted to the interior of the rock block, and more intact rock participated in the bearing failure.

Influence of the prestressed bolt density on the strength of jointed rock blocks

Figure 8 shows the stress–strain curves of rock blocks with a joint dip angle of 60° under different prestressed bolt densities. It is observed that with growing prestressed bolt density, the strengths of the jointed rock blocks are 4.4, 8.1, 9.0 and 10.6 MPa, respectively.

The strength of the anchored rock block with a single-row prestressed bolt is approximately 84.1% greater than that of the rock block without a prestressed bolt, and relative to the single-row anchored rock block peak strength, the double- and triple-row anchored rock blocks show further increases in the peak strength by 11.1% and 30.8%, respectively. The application of a single-row prestressed bolt system significantly enhances the strength of the anchored rock block, whereas the further application of a double-row prestressed bolt system does not significantly improve the strength of the anchored rock block; however, the application of a three-row prestressed bolt system again significantly improves the strength. This phenomenon is linked to the failure mode of the rock block. When a rock block with a joint dip angle of 60° is subjected to a vertical load, the rock pillar in the joint normal direction slips in the joint dip direction, and the rock bridge in the joint dip direction hinders the displacement of the rock pillar, leading to shear slip failure of the whole rock block (Fig. 9). It is clear from Fig. 9 that the strength of rock block is related to the failure area of rock bridge. The calculation formula of the damaged area of the rock bridge is shown in Eq. (1).

$$A = aL \tag{1}$$

Where A = Failure area of rock bridge; a = Aperture of fracture; L = Length of fracture.

The failure area of unanchored jointed rock block is mainly composed of three rock bridges with greater failure degree (shown by rectangular region in Fig. 9a). Compared with the unanchored rock block, the anchored with the single-row prestressed bolt system is more broken because the prestressed bolt system mobilizes more intact rock to participate in the load (shown by yellow circle in Fig. 9b), the failure area of rock bridge increased by about 75%, so that the strength of the rock block is remarkably improved. The anchoring mechanism of the anchored rock block with the double-row bolt system is the same as that of the single-row bolt system. Increasing

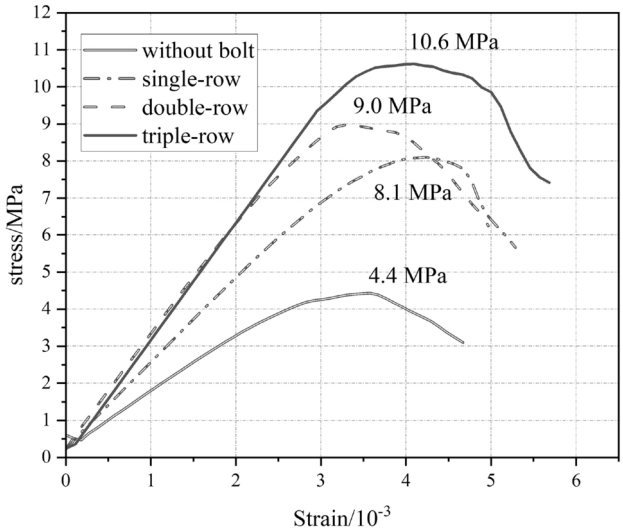

Fig. 8. Stress–strain curves of jointed rock blocks under different prestressed bolt densities.

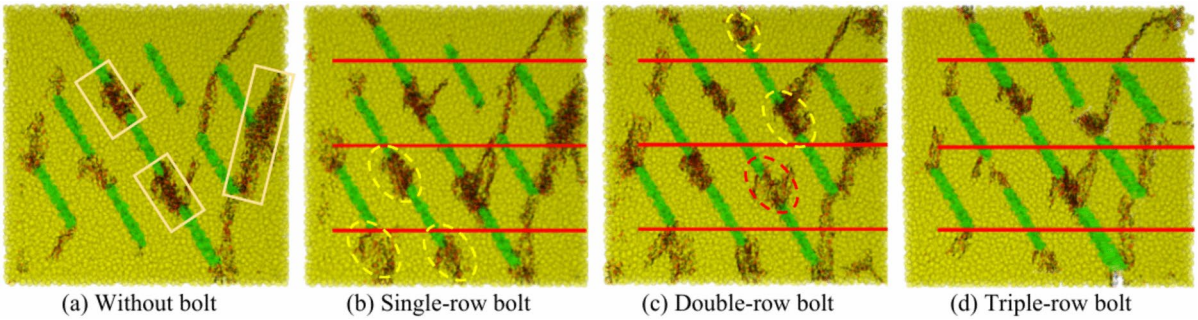

Fig. 9. Particle displacement and failure mode in the 60° jointed rock block.

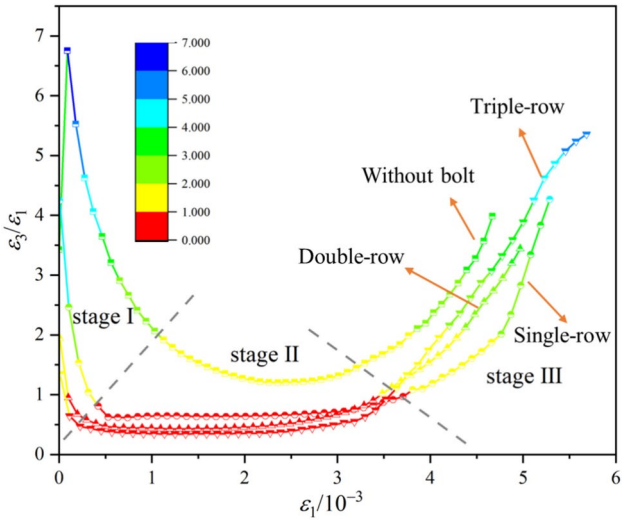

Fig. 10. Variation of $\varepsilon_3/\varepsilon_1$ of with ε_1 for different jointed rock masses with different bolt densities.

the density of the prestressed bolt only adds two rock bridges to participate in the load bearing (shown by yellow circle in Fig. 9c), and failure degree to one rock bridge was reduced (shown by red circle in Fig. 9c), the failure area of the rock bridge only increased by 14%, and has a limited effect on the strength of the rock block. However, the anchored rock block with the three-row prestressed bolt system can bear the tensile shear load at the fracture plane due to the high density of the prestressed bolt so that the rock block on the right side of the model keeps sliding along the bolt and maintains stability. The load is mainly borne by the prestressed bolt, and the overall fracture degree of the rock block is reduced (Fig. 9d), so that the strength of the rock mass is significantly improved again.

Influence of the prestressed bolt density on the deformation properties of jointed rock blocks

To intuitively show the influence of the prestressed bolt system support on the deformation properties of the rock block, the strain of the free surface (ε_3) is normalized by the strain of the loading wall (ε_1). Then, $\varepsilon_3/\varepsilon_1$ is plotted versus ε_1 in Fig. 10. It is important to note that if $\varepsilon_3/\varepsilon_1$ is greater than 1.0, the rock block's horizontal deformation is better than the vertical deformation, which usually means that the rock block experiences sliding failure along the joint plane. If $\varepsilon_3/\varepsilon_1$ is less than 1.0 (red dot in Fig. 10), the rock block volume decreases, and the rock block carrying capacity increases. The whole curve can be divided into three stages, I, II and III, corresponding to the stress release stage, the relatively stable deformation stage and the unstable failure stage, respectively.

In stage I, the initial stress release results in the elastic deformation of the unanchored jointed rock block. In this stage, the vertical strain ε_1 is also small because of the small normal stress. Therefore, the $\varepsilon_3/\varepsilon_1$ values are large and distributed between 3.0 and 6.9 under different prestressed bolt systems in stage I. With the rapid release of elastic strain from the jointed rock block, $\varepsilon_3/\varepsilon_1$ decreases significantly. The application of a prestressed bolt system is equivalent to applying a certain confining pressure on the free surface, which has a certain hindering effect on the stress release at the free surface, resulting in a small strain on the free surface. With increasing prestressed bolt system density, the prestress exerted on the free surface of the anchored rock block increases, $\varepsilon_3/\varepsilon_1$ decreases, ranging from 0.8 to 4.2, and the stress release period decreases.

In stage II, with increasing ε_1, the number of microfractures in the rock block model gradually increases, and the deformation of the rock block model becomes relatively stable. The curve of the unanchored rock block

does not contain a linear segment but rather presents a smooth arc, and the lowest value is greater than 1.0, indicating that the jointed rock block is always in an unstable state and undergoes unstable deformation in stage II. Single-row, double-row and triple-row prestressed bolt systems can improve the unstable deformation state of the unanchored rock block and achieve a stable value for the $\varepsilon_3/\varepsilon_1$ ratio of the rock block model. With increasing prestressed bolt system density, $\varepsilon_3/\varepsilon_1$ gradually decreases. Stage II corresponds to the elastic stage of the stress–strain curve, and $\varepsilon_3/\varepsilon_1$ decreases with larger deformation modulus. The $\varepsilon_3/\varepsilon_1$ for the single-row prestressed bolt system is approximately 0.6, the $\varepsilon_3/\varepsilon_1$ for the double-row prestressed bolt system is approximately 0.4, and the $\varepsilon_3/\varepsilon_1$ for the three-row prestressed bolt system is approximately 0.3.

In stage III, the curve rises rapidly. The preexisting joints of the rock block model are extended and connected with the microfractures to develop a macroscopic fracture plane. The fragmentation blocks break off and slip along the fracture plane, leading to a large displacement change in the direction of the free surface. The application of the prestressed bolt system slows down the curve rise in stage III, indicating that the prestressed bolt system can advance the ductile failure of the rock block.

Discussion

The above research results indicate that increasing the prestress of the bolt can greatly reduce the lag of the full action of the bolt, and can make the bolt play its role earlier. Moreover, the increase of prestressed bolt density is equivalent to confining pressure applied on the free surface of rock mass, which can effectively control the sliding deformation of rock mass. Meanwhile, increasing the prestress and density of prestressed bolt can improve the strength of rock mass, but the effect of improving is gradually weakened. Figure 11 shows the improvement rate of rock mass strength induced by prestress of bolt. When the prestress of the bolt is 0.2 kN, the strength of the rock mass is increased by 57.8%. When the prestress of bolt is increased to 0.4 kN and 0.6 kN again, the strength of rock mass is increased by 19.9% and 6.5% respectively. Figure 12 shows the improvement rate of prestressed bolt density on rock mass strength. When a single-row prestressed bolt is employed to rock mass, the strength of rock mass increases by 84.1% compared with that without bolt. When double-row and triple-row bolts are applied again, the strength of rock mass increases by 11.1% and 17.8%, respectively. It is clear that when the prestressed bolt is added to the double-row, the improvement effect on the strength of the rock mass shows a weakening trend, because the main function of the prestressed bolt with low density is to mobilize more intact rock to participate in the bearing, with the increase of bolt density, less and less intact rock can be mobilized. However, for the triple-row anchored rock mass with large bolt density, the strength of the rock mass increases again because the prestressed bolt bears the main load.

Through the quantitative analysis of the performance improvement of prestressed bolt on rock mass, it can be found that the prestressed bolt on the rock mass is limited. When the prestress and density of bolt reach a certain degree, the strength of rock mass is only increased by 10% when the prestress and density of bolt are doubled. However, it is very expensive to improve the prestress and density of the bolt in actual engineering, and there is no need for the strength of the rock mass to be improved to a very high degree, the stability of the surrounding rock can only meet the design requirements. Therefore, it is indispensable to optimize the design parameters of tunnel support scheme based on the strength improvement rate of rock mass and cost.

Conclusions

In this study, we develop a simulation method for a prestressed bolt in a 3D particle flow numerical program, establish a numerical model of an anchored rock block, and the performance improvement of a prestressed bolt system for a rock block is quantitatively discussed and explored. The main conclusions are as follows:

(1) Adding bolt does not change the original failure mode of jointed rock mass, which is still dominated by shear slip failure. Under the action of anchoring, microfractures of single-row and double-row anchored rock mass fully develop, the total amount of microfractures increases, and more intact rocks participate in the load

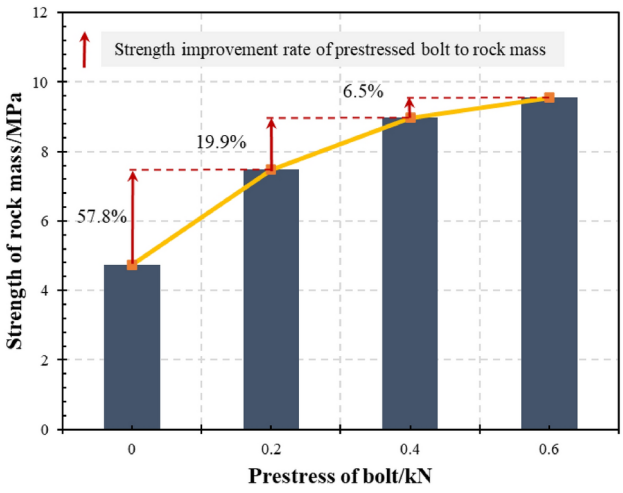

Fig. 11. Relationship between prestress of bolt and strength of rock mass.

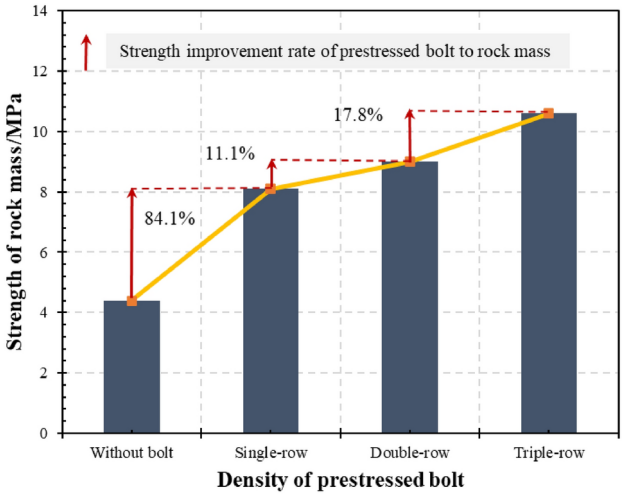

Fig. 12. Relationship between density of prestressed bolt and strength of rock mass.

bearing. The microfractures of the rock mass in triple-row are less developed, and the load is mainly borne by the bolt.

(2) The rock block with a joint dip angle of 60° mainly experiences shear slip failure. The single-row prestressed bolt system can mobilize more intact rock to participate in the load, which can increase the strength of the rock mass by 84.1%. And an increase in the density of the prestressed bolt leads to a change in the anchoring mechanism of the rock block. The triple-row prestressed bolt system mainly bears the tensile shear load at the fracture surface, increasing the strength of the rock mass anchored by the single-row prestressed bolt by 30.8%. The $\varepsilon_3/\varepsilon_1$ ratio can be used as the criterion for whether the rock block maintains stable deformation during the loading process. The $\varepsilon_3/\varepsilon_1$ value of the anchored rock block is lower than that of the unanchored rock block and is consistently less than 1.0 in stage II.

(3) The prestress and density of prestressed bolt have limited effect on the performance improvement of tunnel surrounding rock mass. When the prestress and density of bolt reach a certain degree, the strength of rock mass is only increased by 10% when the prestress and density of bolt are doubled. At this time, the support cost of tunnel surrounding rock mass is much higher than the strength improvement rate.

Data availability

Data sets generated during the current study are available from the corresponding author on reasonable request.

Received: 18 December 2024; Accepted: 24 February 2025
Published online: 28 February 2025

References

1. Jing, H. W. et al. Theoretical and technical progress of stability control of broken rock zone of deep roadway surrounding rock. *J. Min. Saf. Eng.* **37**(03), 429–442 (2020).
2. Fan, W. C. et al. Experimental and numerical investigation on crack mechanism of folded flawed rock-like material under uniaxial compression. *Eng. Geol.* **291**, 106210 (2021).
3. Kränkel, T., Lowke, D. & Gehlen, C. Prediction of the creep behaviour of bonded anchors until failure–A rheological approach. *Constr. Build. Mater.* **75**, 458–464 (2015).
4. Puigvert, F., Gil, L. & Escrig, C. Stress relaxation analysis of adhesively bonded anchorages for CFRP tendons. *Constr. Build. Mater.* **66**(15), 313–322 (2014).
5. Chen, J. H. & Li, D. Q. Numerical simulation of fully encapsulated rock bolts with a tri-linear constitutive relation. *Tunn. Undergr. Sp. Tech.* **120**, 104265 (2022).
6. Zhu, B., Zhou, C. B. & Jiang, N. Dynamic characteristics and safety control of mortar bolts under tunnel blasting vibration loads. *Tunn. Undergr. Sp. Tech.* **135**, 105005 (2023).
7. Song, Y., Fan, B. & Wang, H. P. Research on shear mechanics model of anchored-jointed rock mass considering normal stress and rock strength. *Chin. J. Rock. Mech. Eng.* **42**(06), 1325–1335 (2023).
8. Liu, Q. S. et al. Study on shear mechanical properties of sandstone, marble and granite after anchoring. *Chin. J. Rock. Mech. Eng.* **37**(S2), 4007–4015 (2018).
9. He, M. et al. Experimental study on the shear performance of quasi-NPR steel bolted rock joints. *J. Rock. Mech. Geotech.* **15**(2), 350–362 (2023).
10. He, M. et al. Experimental study on influence of host rock strength on shear performance of Micro-NPR steel bolted rock joints. *Int. J. Rock Mech. Min. Sci.* **159**, 105236 (2022).
11. Ding, S. X. et al. Analysis on bolt performance during deformation process of anchorage containing a weak interlayer. *J. Min. Saf. Eng.* **34**(06), 1094–1102 (2017).
12. Teng, J. Y. et al. Mechanical behaviors of anchored bedding rock under uniaxial compression. *Rock. Soil. Mech.* **38**(07), 1974–1982 (2017).
13. Zhang, B. et al. Bolting effect and failure modes of jointed rock masses with cross-cracks. *Chin. J. Rock. Mech. Eng.* **33**(05), 996–1003 (2014).

14. Zhang, N. et al. Experimental study of reinforced effect of bolt in 3D surface fractured specimens under uniaxial compression. *Rock. Soil. Mech.* **32**(11), 3288–3294 (2011).
15. Wu, X. Z., Jiang, Y. J. & Li, B. Influence of joint roughness on the shear behaviour of fully encapsulated rock bolt. *Rock. Mech. Rock. Eng.* **51**(3), 953–959 (2018).
16. Wang, W. J. et al. Experimental study on mechanical properties of anchorage body and on anchorage mechanism. *J. China. Coal. Soc.* **45**(01), 82–89 (2020).
17. Wang, W. J. et al. Simulation on anchorage mechanism of rock mass. *J. China. Coal. Soc.* **48**(01), 177–184 (2023).
18. Wang, G. H. et al. Mechanism analysis of pre-stressed bonded rock bolt controlling the deformation in joint surrounding rocks. *J. China. U. Min. Technol.* **50**(01), 60–68 (2021).
19. Liu, Q. S. et al. Experimental study and mechanism analysis of influence of bolt anchoring on shear properties of jointed rock mass. *Rock. Soil. Mech.* **38**(S1), 27–35 (2018).
20. Wang, X. G., Zhao, Y. F., Nie, Y., Lin, X. C. & Sun, X. S. The shear resistance mechanism of prestressed anchor cables in slope reinforcement. *Int. J. Rock Mech. Min. Sci.* **170**, 105520 (2023).
21. Meng, B. et al. Experimental study of deformation and failure characteristics of anchorage unit in fractured surrounding rocks. *Chin. J. Rock. Mech. Eng.* **32**(12), 2497–2505 (2013).
22. Zhang, Y. et al. Study on dynamic mechanical properties of prestressed bolt group under impact load. *Structures.* **67**, 107024 (2024).
23. Jing, H. W. et al. An experimental study on anchorage strength and deformation behavior of large-scale jointed rock mass. *Tunn. Undergr. Sp. Tech.* **43**, 184–197 (2014).
24. Sun, P. P. et al. Optimally designed shotcrete material and its cooperating performance when integrated with sandstone. *Constr. Build. Mater.* **249**, 118742 (2020).
25. Li, P. et al. Study on bonding performance and load transfer model between polyurethane anchor bolts and silty soil. *Constr. Build. Mater.* **384**, 131335 (2023).
26. Yang, X. X. et al. Numerical simulation of a jointed rock block mechanical behavior adjacent to an underground excavation and comparison with physical model test results. *Tunn. Undergr. Sp. Tech.* **50**, 129–142 (2015).
27. Guo, J. W. et al. Development of a shear strength model for a rock mass containing a complex fracture system based on direct shear tests: a case study. *B. Eng. Geol. Environ.* **83**(1), 34 (2024).
28. Yang, X. X. & Qiao, W. G. Numerical investigation of the shear behavior of granite materials containing discontinuous fractures by utilizing the flat-fracture model. *Comput. Geotech.* **104**, 69–80 (2018).
29. Yang, W., Wang, X., Ivanović, A. & Zhang, X. Coupled analytical solutions for circular tunnels considering rock creep effects and time-dependent anchoring forces in prestressed bolts. *Tunn. Undergr. Sp. Tech.* **134**, 104954 (2023).
30. Yu, W., Wang, B., Zi, X. & Dong, J. Elastoplastic coupling analysis of surrounding rock-prestressed yielding anchor bolts/cables based on unified strength theory. *Tunn. Undergr. Sp. Tech.* **143**, 105491 (2024).
31. Li, P. et al. Design principles of prestressed anchors for tunnels considering bearing arch effect. *Comput. Geotech.* **156**, 105307 (2023).
32. Jing, H. W. et al. Macroscopic and mesoscopic evolution characteristics of surrounding rock of rectangular bottom coal roadway in deep during failure. *J. Min. Saf. Eng.* **39**(01), 82–93 (2022).
33. Wang, X. Q. et al. Analysis of pressure arch formation and rock bolt function in gravel bolting. *J. China. Coal. Soc.* **46**(10), 3139–3147 (2021).
34. Sun, X. M., Zhao, W. C., Shen, F. X., Zhang, Y. & Jiang, M. Study on failure mechanism of deep soft rock roadway and high prestress compensation support countermeasure. *Eng. Fail. Anal.* **143**, 106857 (2023).
35. Wang, J., Liu, P., He, M. C., Tian, H. Z. & Gong, W. L. Mechanical behaviour of a deep soft rock large deformation roadway supported by NPR bolts: a case study. *Rock. Mech. Rock. Eng.* **56**(12), 8851–8867 (2023).

Acknowledgements

The research reported in this manuscript was financially supported by the National Natural Science Foundation of China (Grant No. 52274088) and the Natural Science Foundation of Shandong Province, China (Grant No. ZR2022ME056).

Author contributions

X.X. and H.Y. wrote the main manuscript text; X.X. , H.Y. and M.M. made investigation; H.Y. prepared Figs. 1–6 and J.W. prepared 10–12 and M.M. prepared Figs. 7–9; H.Y.wrote the original draft; X.X. and J.W. made reviewing and editing; All authors reviewed the manuscript.

Declaration

Competing interests

The authors declare no competing interests.

Additional information

Correspondence and requests for materials should be addressed to J.G.